

A non-Hermitian approach for edge/surface states in bounded systems

Huiping Wang(王会平), Li Ren(任莉), Xiuli Zhang(张修丽), and Liguo Qin(秦立国)
Citation: Chin. Phys. B, 2025, 34 (**12**): 127304. DOI: 10.1088/1674-1056/ade1c1
http://cpb.iphy.ac.cn; http://iopscience.iop.org/cpb

What follows is a list of articles you may be interested in

Doping-induced magnetic and topological transitions in $Mn_2X_2Te_5$ (X = Bi, Sb) bilayers

Wei Chen(陈威), Chuhan Tang(唐楚涵), Chao-Fei Liu(刘超飞), and Mingxing Chen(陈明星)
Chin. Phys. B, 2025, 34 (**9**): 097304. DOI: 10.1088/1674-1056/ade4af

Random flux manipulating topological phase transitions in Chern insulators

Jinkun Wang(王锦坤) and Wu-Ming Liu(刘伍明)
Chin. Phys. B, 2025, 34 (**6**): 067301. DOI: 10.1088/1674-1056/adc36a

Merging and separation of polarization singularities in complex lattices

Mengyao Wang(王梦瑶), Tian Shi(石天), Luhui Ning(宁鲁慧), Peng Liu(刘鹏), Liangsheng Li(李粮生), and Ning Zheng(郑宁)
Chin. Phys. B, 2025, 34 (**3**): 037303. DOI: 10.1088/1674-1056/ada9da

Higher-order topology in twisted multilayer systems: A review

Chunbo Hua(花春波) and Dong-Hui Xu(许东辉)
Chin. Phys. B, 2025, 34 (**3**): 037301. DOI: 10.1088/1674-1056/ada885

Topological hierarchy matters–topological matters with superlattices of defects

Jing He(何敬), Su-Peng Kou(寇谡鹏)
Chin. Phys. B, 2016, 25 (**11**): 117310. DOI: 10.1088/1674-1056/25/11/117310

A non-Hermitian approach for edge/surface states in bounded systems

Huiping Wang(王会平)[†], Li Ren(任莉), Xiuli Zhang(张修丽), and Liguo Qin(秦立国)

School of Mathematics, Physics and Statistics, Shanghai University of Engineering Science, Shanghai 201620, *China*

(Received 12 March 2025; revised manuscript received 4 June 2025; accepted manuscript online 6 June 2025)

We suggest and develop a novel approach to determine edge/surface states in bounded systems based on the bulk Hamiltonian of their corresponding unbounded counterparts, where the k-space is extended to the complex k-one. This approach allows us to obtain simple conditions for the existence of edge/surface states in bounded systems. Our analysis also demonstrates that the emergence of such edge/surface states, which are intrinsically linked to the characteristics of system boundaries, cannot manifest without appropriate boundary conditions dictated by the necessity for wave function convergence. In order to demonstrate our method in action, we apply it to study some examples of non-topological and topological edge/surface states. We hope our discussion helps you gain a clearer and more intuitive understanding of the bulk–boundary correspondence.

Keywords: edge/surface states, bounded systems, bulk–boundary correspondence

PACS: 73.20.At, 61.50.Ah, 73.22.Dj, 02.10.Yn

DOI: 10.1088/1674-1056/ade1c1 **CSTR:** 32038.14.CPB.ade1c1

1. Introduction

The study of edge/surface states in condensed matter systems has been a focus of intense research interest, not only for their fundamental scientific importance but also due to their powerful applications in future devices. The investigation of non-topological edge, surface and interface states in ferroelectric materials has emerged as a prominent research focus. This effort seeks to elucidate the conductive properties of ferroelectric domain walls,[1,2] driven by their critical applications in next-generation electronic devices, exemplified by non-volatile ferroelectric random access memories.[3] However, the topological phase of matter has garnered significant attention owing to its exotic properties. Notably, topological band theory has served as a cornerstone in revealing diverse classes of topological phases through combining the principles of band theory and topology.[4–7] One of the most intriguing phenomena in topological phases is the bulk–boundary correspondence, which signifies edge states induced by the topology of the bulk.[8–10] These topological edge states emerge regardless of other details of systems and are sources of anomalous behaviors. Consequently, they form an exciting playground for technological applications. For example, topological insulators have emerged as viable candidates for implementing quantum computing qubits,[11,12] while also demonstrating enhanced lasing efficiency and harmonic generation capabilities in photonic systems.[13]

Although the study of edge/surface states is crucial for investigating certain fundamental physical phenomena, we still encounter challenges in finding analytical solutions. To derive analytical expressions for edge/surface states in bounded systems, several established approaches have been developed to address this challenge, including partial differential equations in the continuum limit,[14] Green's function method, and transfer matrix method. However, these methods often encounter limitations when applied to complex Hamiltonians. Therefore, it is common to integrate experimental techniques, such as angle-resolved photoemission spectroscopy and electrical transport measurements, with numerical approaches, such as the exact diagonalization method, to carry out comprehensive investigations into the behavior of edge/surface states.

In topological systems, the characteristics of edge/surface states are predominantly understood through topological invariants derived from bulk states.[15–17] It is precisely because the bulk–boundary correspondence defines the relation between bulk topological invariants and the number of edge/surface states. It is worthwhile to rephrase the physics that the analytical solutions of edge/surface states in a bounded system can be directly derived from the bulk Hamiltonian of its corresponding unbounded system. The bulk–boundary correspondence may offer a simpler approach to calculating the analytical solutions of edge/surface states for some bounded systems, potentially avoiding the complexity involved in directly solving the eigenvalue equation of the bounded system. Therefore, in the present paper, we will elucidate such physics and develop a novel approach to characterize edge/surface states in bounded systems derived from the bulk Hamiltonian of their unbounded counterparts. This is achieved by extending the k-space to the complex k-one, thereby transforming the original

[†]Corresponding author. E-mail: hp_wang@fudan.edu.cn

© 2025 Chinese Physical Society and IOP Publishing Ltd. All rights, including for text and data mining, AI training, and similar technologies, are reserved.

Hermitian Hamiltonian into its non-Hermitian counterpart.[18] It is worth noting that we introduce non-Hermitian Hamiltonians mainly to calculate edge/surface states and their corresponding eigen-energies. Through this approach, we obtain simple conditions for the existence of edge/surface states in bounded systems. Our analysis reveals that the appearance of these edge/surface states, which are tied to the properties of system boundaries, is contingent upon the imposition of suitable boundary conditions that ensure wave function convergence. Subsequently, in order to verify our viewpoint to be reasonable and acceptable, we will give some examples of non-topological and topological states.

2. The novel approach for edge/surface states

Now, we propose an independent approach for addressing edge/surface states in a bounded system, derived from the bulk Hamiltonian of its corresponding unbounded system. For the sake of discussion, we initially assume the existence of a general Hamiltonian $H(\boldsymbol{k})$, which is represented in momentum space $\boldsymbol{k}$ and an $n\times n$ ($n\geq 1$) matrix that depends on the number of band mixings considered near the Fermi surface. Then we have

$$H(\boldsymbol{k})\Psi_l(\boldsymbol{k}) = E_l(\boldsymbol{k})\Psi_l(\boldsymbol{k}), \tag{1}$$

here $\{\Psi_l(\boldsymbol{k}), E_l(\boldsymbol{k}) : l = 1,2,\ldots,n\}$ are the eigenstates and eigenvalues of Hamiltonian $H(\boldsymbol{k})$, $\{\boldsymbol{k}, E_l(\boldsymbol{k})\}$ are real and $\boldsymbol{k}$ is within the Brillouin zone. In the position space $\boldsymbol{r}$, $\Psi_l(\boldsymbol{k})$ can be represented as $\Psi_{l,\boldsymbol{k}}(\boldsymbol{r}) \sim \mathrm{e}^{\mathrm{i}\boldsymbol{k}\cdot\boldsymbol{r}}$, which means the electron wave extended in the bulk. In the subsequent discussion, we will explore the approach for deriving edge/surface states from the aforementioned Hamiltonian $H(\boldsymbol{k})$. If we consider the boundary embedded within a certain direction of the unbounded system, the momentum $\boldsymbol{k}$ can be decomposed into two components: $\boldsymbol{k}_{\shortparallel}$ (parallel to the boundary) and $\boldsymbol{k}_{\perp}$ (perpendicular to the boundary). Consequently, equation (1) can be reformulated as

$$H(\boldsymbol{k}_{\shortparallel},\boldsymbol{k}_{\perp})\Psi_l(\boldsymbol{k}_{\shortparallel},\boldsymbol{k}_{\perp}) = E(\boldsymbol{k}_{\shortparallel},\boldsymbol{k}_{\perp})\Psi_l(\boldsymbol{k}_{\shortparallel},\boldsymbol{k}_{\perp}). \tag{2}$$

By extending the real $\boldsymbol{k}_{\perp}$-space to the complex $\boldsymbol{k}_{\perp}$-one, the Hamiltonian $H(\boldsymbol{k}_{\shortparallel},\boldsymbol{k}_{\perp})$ becomes non-Hermitian[18] and we can examine the behavior of edge/surface states in this particular boundary direction. For some real energy $E = E(\boldsymbol{k}_{\shortparallel},\boldsymbol{k}_{\perp})$, we solve Eq. (2) and can have acceptable solutions $\boldsymbol{k}_{\perp} = \boldsymbol{k}_r + \mathrm{i}\boldsymbol{k}_i$ where $(\boldsymbol{k}_r,\boldsymbol{k}_i)$ are real and $\boldsymbol{k}_i \neq 0$, then edge/surface states may accommodate in such a bounded system because the presence of $\boldsymbol{k}_{\perp} = \boldsymbol{k}_r + \mathrm{i}\boldsymbol{k}_i$ is one of the necessary conditions for the appearance of edge/surface states. It is noteworthy that $\{\mathrm{e}^{\mathrm{i}\boldsymbol{k}_{\perp}\cdot\boldsymbol{r}}, \mathrm{e}^{-\mathrm{i}\boldsymbol{k}_{\perp}\cdot\boldsymbol{r}}\}$ invariably coexist.[19–21] Due to the convergence of the wave function, when all terms $|\mathrm{e}^{\mathrm{i}\boldsymbol{k}_{\perp}\cdot\boldsymbol{r}}|$ are less than 1, the edge/surface states localize at the left boundary; conversely, when all terms $|\mathrm{e}^{-\mathrm{i}\boldsymbol{k}_{\perp}\cdot\boldsymbol{r}}|$ exceed 1, they localize at the right boundary.

The second essential constraint is that all $\boldsymbol{k}_i$ values derived from identical boundary conditions must share the same sign, in addition to their magnitudes, for a given $\boldsymbol{k}_r$. To enhance comprehension of the second constraint, we provide a detailed explanation through a one-dimensional (1D) example by means of the transfer matrix method (TMM).[22,23] For a monoatomic one-dimensional chain with the perfect surface under the nearest neighbor hopping approximation, the quantum dynamical equations can be rigorously derived in the following form:

$$\begin{cases} E\psi_n = t(\psi_{n-1} + \psi_{n+1}), \\ E\psi_1 = t\psi_2, \quad n > 1, \end{cases} \tag{3}$$

where the boundary is set at the 1st layer and $\{\psi_n : n \leq 0\}$. With the help of TMM, we can have

$$\begin{pmatrix} \psi_{n+1} \\ \psi_n \end{pmatrix} = U \begin{pmatrix} \Gamma_1\beta_-^n \\ \Gamma_2\beta_+^n \end{pmatrix} \psi_1, \tag{4}$$

where U^{-1} and U can be found,[23] $\Gamma_1 = U_{11}^{-1}\alpha + U_{12}^{-1}$, $\Gamma_2 = U_{21}^{-1}\alpha + U_{22}^{-1}$, $\beta_{\pm} = (\alpha \pm \sqrt{\alpha^2-4})/2$, $\alpha = E/t$, and $\beta_-\cdot\beta_+ = 1$. When $|\alpha| \leq 2$, we have $|\beta_-| = |\beta_+| = 1$ which corresponds to the extended bulk states. Here we only focus on $\alpha > 2$ since the demonstration is similar for $\alpha < -2$. When $\alpha > 2$, $\beta_+ > 1$ and $0 < \beta_- < 1$. If there exist edge states, we must impose the conditions due to the wave function convergence

$$\begin{cases} \Gamma_1 = U_{11}^{-1}\alpha + U_{12}^{-1} \neq 0, \\ \Gamma_2 = U_{21}^{-1}\alpha + U_{22}^{-1} = 0. \end{cases} \tag{5}$$

After some detailed calculations, we can find when $U_{21}^{-1}\alpha + U_{22}^{-1} = 0$, then the relation $U_{11}^{-1}\alpha + U_{12}^{-1}$ is also zero. As a result, no surface states can emerge in such cut materials. Thus, we focus on edge/surface states that they decay exponentially from the same boundary conditions.

In the field of topological states of matter, it is widely acknowledged that their existence remains robust against specific details, with the exception of band topology. However, recent theoretical studies have highlighted the crucial role of boundaries in topological crystalline insulators.[24] Moreover, the edges of two-dimensional (2D) materials exhibit significant functionalities and distinct properties due to the presence of dangling chemical bonds and the loss of symmetry. Recent studies have demonstrated that the electronic and magnetic properties of honeycomb crystalline graphene and transition metal dichalcogenides are strongly influenced by the atomic configurations at their edges.[25] However, in practical materials, their size is always finite. Therefore, if the behavior of edge/surface states exhibits the fundamental correlation with

the boundaries, the third requirement is that both the left and right boundary conditions must be fulfilled. The third requirement is similar to Eqs. (5) and (6) in the previous study.[21] It is worth noting that, based on the calculation results of non-Hermitian Hamiltonians, it is found that for the edge/surface state expression in the bounded system, their exponential decay coefficients are not always unique; there may be multiple values. The parameter λ in Eqs. (5) and (6) of the previous study[21] should be taken as the maximum value of these exponential decay coefficients. In the subsequent sections, we utilize our methodology to examine various instances of edge/surface states, encompassing both non-topological and topological systems.

3. Example I: Single-layer graphene with the nearest neighbor hopping

At the level of the nearest neighbor hopping approximation and in the basis of $(c_{k\mathrm{A}}, c_{k\mathrm{B}})$, its Hamiltonian reads (see Fig. 1(a))

$$H = \begin{pmatrix} 0 & m \\ m^* & 0 \end{pmatrix}, \tag{6}$$

where $m = t(\mathrm{e}^{\mathrm{i}k_x a/\sqrt{3}} + 2\cos(k_y a/2)\,\mathrm{e}^{-\mathrm{i}k_x a/2\sqrt{3}})$ and t is the nearest neighbor hopping amplitude. By diagonalizing H, we can reach the bulk energy spectrum $E_\pm(k) = \pm|m|$. Based on the approach we have proposed, we will systematically investigate the behavior of edge states under various boundary conditions. Firstly, we take into account zero-energy edge states in the zigzag edged graphene where k_y is a good quantum number, the condition $E_\pm(k) = 0$ has the acceptable solutions $\mathrm{e}^{\sqrt{3}\mathrm{i}k_x a/2} = -2\cos(k_y a/2)$ and $\mathrm{e}^{-\sqrt{3}\mathrm{i}k_x a/2} = -2\cos(k_y a/2)$ where $m = 0$ and $m^* = 0$ are used respectively. According to the convergence of the wave function, if edge states localize at the left (right) boundary, we must restrict the exponential decay coefficient $|\mathrm{e}^{\sqrt{3}\mathrm{i}k_x a/2}| < 1$ ($|\mathrm{e}^{-\sqrt{3}\mathrm{i}k_x a/2}| < 1$), that is, $|2\cos(k_y a/2)| < 1$. Since the behavior of edge states is fundamentally dependent on the boundary conditions, we must confine $k_y a \in (2\pi/3, \pi)$ and $(-\pi, -2\pi/3)$ in terms of the third requirement, which shows a good agreement with the result.[23] To verify the correctness of the proposed approach, we compare the analytical results with the numerical results obtained through the exact diagonalization method and find that they are completely consistent, as shown in Fig. 1(b). Secondly, we focus on zero-energy edge states in the armchair edged graphene where k_x is a good quantum number. When $E_\pm(k) = 0$, we obtain the legitimate solutions

$$\mathrm{e}^{\mathrm{i}k_\pm a/2} = \beta_\pm = \left\{ -\mathrm{e}^{\sqrt{3}\mathrm{i}k_x a/2} \pm \sqrt{\mathrm{e}^{\sqrt{3}\mathrm{i}k_x a} - 4} \right\}/2,$$
$$\mathrm{e}^{-\mathrm{i}k_\pm a/2} = \gamma_\pm = \left\{ -\mathrm{e}^{-\sqrt{3}\mathrm{i}k_x a/2} \pm \sqrt{\mathrm{e}^{-\sqrt{3}\mathrm{i}k_x a} - 4} \right\}/2$$

as shown in Figs. 1(c) and 1(d), where $m = 0$ and $m^* = 0$ are employed respectively. Figures 1(c) and 1(d) show that one of $|\beta_\pm|$ ($|\gamma_\pm|$) is always greater than 1 for different k_x. There are no zero-energy edge states due to the wave function convergence, which is in accord with the analysis.[26] With the help of the exact diagonalization method, the behavior of zero-energy edge states in the armchair edged graphene is found to be consistent with our demonstration, as shown in Fig. 1(e). Finally, we discuss the non-zero-energy edge states in the zigzag edged graphene. When $E_\pm(k) \neq 0$, we obtain $\mathrm{e}^{\pm\sqrt{3}\mathrm{i}k_x a} = \delta_\pm = \{-b(k_y) \pm \sqrt{b^2(k_y) - 16\cos^2(k_y a/2)}\}/\{4\cos(k_y a/2)\}$ with $b(k_y) = 1 + 4\cos^2(k_y a/2) - E^2/t^2$ and $\cos(k_y a/2) \neq 0$. To make our demonstration simple and understandable, we depict the behavior of edge states when $E = 2.5t$ as shown in Fig. 1(f).

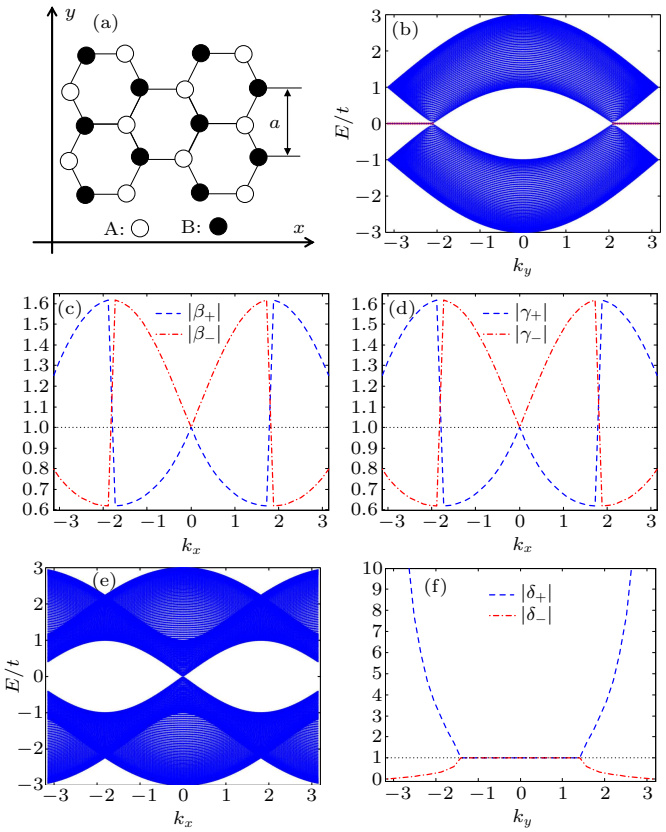


Fig. 1. (a) The schematic illustration of the lattice structure of graphene with the parameter $a = 1$. (b) The energy spectrum of edge states in the zigzag-edged graphene got by the exact diagonalization method (blue dash-line) and our proposed approach (red dash-line). In our proposed approach (red dash-line), the existence of edge states results from the exponential decay coefficient $|\mathrm{e}^{\pm\sqrt{3}\mathrm{i}k_x a/2}| < 1$ and the fulfillment of the third requirement. Panel (c) shows one of $|\beta_\pm|$ is always greater than 1 for different k_x. There are no zero-energy edge states due to the wave function convergence in the armchair edged graphene. Panel (d) presents that one of $|\gamma_\pm|$ is always greater than 1 for different k_x, and zero-energy edge states are not allowed due to the wave function convergence in the armchair edged graphene. (e) The dispersion relation of edge states in the armchair edged graphene reached in terms of the exact diagonalization method (blue dash-line) and our proposed approach (red dash-line). Edge states do not exist in our proposed approach, since one of the absolute values of all decay coefficients derived from the same boundary is always greater than 1. Panel (f) shows $|\delta_-|$ for some regions of k_y is less than 1, thus there might be non-zero-energy edge states localized at the right boundary with the energy $E = 2.5t$.

From Fig. 1(f), we observe that $|\delta_-|$ for certain regions of k_y is less than 1, this suggests the potential existence of non-zero-energy edge states localized at the right boundary.[23] Nevertheless, given that the behavior of edge states is intrinsically tied to the boundary conditions, non-zero-energy edge states are absent in the zigzag-edged graphene according to the third requirement, which is consistent with the study. To check the correctness of our proposed approach, we further investigate the behavior of zero-energy edge states in the armchair edged graphene with the next nearest neighbor hopping interactions, demonstrating that our analytical calculations are in excellent agreement with the results.[27] The specific calculation details are shown in Appendix A.

4. Example II: An AIII class topological insulator and a BDI class topological superconductor

In a 1D system, a Hamiltonian belonging to the AIII class that supports topologically nontrivial fermionic edge states can be expressed in the basis of $(c_{k\uparrow}, c_{k\downarrow})$ as follows:[28]

$$H_{\mathrm{AIII}}(k) = (\Gamma_z - 2t_{\mathrm{s}}\cos k)\,\sigma_z + 2t_{\mathrm{so}}\sin k\sigma_y, \tag{7}$$

where $c_{k\uparrow}$ ($c_{k\downarrow}$) is the annihilation operator of the fermion with spin up (down), t_{s} represents the spin-conserved hopping amplitude, Γ_z is the Zeeman term, t_{so} denotes the spin flip hopping and σ_i is Pauli matrix. Without loss of generality, we postulate that the parameters $\{t_{\mathrm{s}}, t_{\mathrm{so}}, \Gamma_z\}$ take positive real values throughout this analysis. As is well established, the Hamiltonian $H_{\mathrm{AIII}}(k)$ possesses a nontrivial bulk topological invariant $N = 1$ and characterizes a nontrivial topological insulator in the regime where $\Gamma_z < 2t_{\mathrm{s}}$. Subsequently, we demonstrate the methodology for obtaining nontrivial zero-energy edge states at the Γ point using our proposed approach. In the vicinity of the Γ point, equation (7) reduces to

$$H_{\mathrm{AIII}}(k) = \left[\Gamma_z - 2t_{\mathrm{s}} + t_{\mathrm{s}}k^2\right]\sigma_z + 2t_{\mathrm{so}}k\sigma_y. \tag{8}$$

By diagonalizing $H_{\mathrm{AIII}}(k)$ in the vicinity of the Γ point, the exact quasiparticle excitation spectrum is obtained

$$E_\pm = \pm\sqrt{\left(\Gamma_z - 2t_{\mathrm{s}} + t_{\mathrm{s}}k^2\right)^2 + 4t_{\mathrm{so}}^2k^2}. \tag{9}$$

From Eq. (9), it is evident that the condition $E_\pm = 0$ yields $k = 0$ and $\Gamma_z - 2t_{\mathrm{s}} = 0$, which is the phase boundary and indicates the closing of the gap of the system. When $\Gamma_z < 2t_{\mathrm{s}}$, the nontrivial topological phase permits the emergence of localized edge states. For a finite-sized system with hard-wall boundaries implemented at $x = 0$ and $x = L$, the condition $E_\pm = 0$ produces $-\mathrm{i}k_\pm = \delta_\pm = (t_{\mathrm{so}} \pm \sqrt{t_{\mathrm{so}}^2 + t_{\mathrm{s}}(\Gamma_z - 2t_{\mathrm{s}})})/t_{\mathrm{s}}$, derived through the relation $\Gamma_z - 2t_{\mathrm{s}} + t_{\mathrm{s}}k^2 = 2\mathrm{i}t_{\mathrm{so}}k$ and $\mathrm{i}k_\pm = \delta_\pm = (t_{\mathrm{so}} \pm \sqrt{t_{\mathrm{so}}^2 + t_{\mathrm{s}}(\Gamma_z - 2t_{\mathrm{s}})})/t_{\mathrm{s}}$, using the relation $\Gamma_z - 2t_{\mathrm{s}} + t_{\mathrm{s}}k^2 = -2\mathrm{i}t_{\mathrm{so}}k$ besides the real momentum $k = 0$. To determine the edge state localized at the left boundary $x = 0$, it is necessary to solve the corresponding matrix equation

$$\begin{pmatrix} \Gamma_z - 2t_{\mathrm{s}} + t_{\mathrm{s}}k^2 & -2\mathrm{i}t_{\mathrm{so}}k \\ 2\mathrm{i}t_{\mathrm{so}}k & -\left(\Gamma_z - 2t_{\mathrm{s}} + t_{\mathrm{s}}k^2\right) \end{pmatrix}\psi_{\mathrm{L}} = 0. \tag{10}$$

After some calculations, we can find that $\psi_{\mathrm{L}} = [1, 1]$, where we have used the relation $\Gamma_z - 2t_{\mathrm{s}} + t_{\mathrm{s}}k^2 = 2\mathrm{i}t_{\mathrm{so}}k$. Consequently, the edge state localized at the left boundary $x = 0$ is explicitly expressed as $\Psi_{\mathrm{L}} = [1, 1]\,(\mathrm{e}^{-\delta_+ x} - \mathrm{e}^{-\delta_- x})$ where $\delta_\pm$ are derived from the bulk dispersion relations. Analogously, the edge state localized on the right boundary $x = L$ is given as $\Psi_{\mathrm{R}} = [-1, 1]\,(\mathrm{e}^{\delta_+(x-L)} - \mathrm{e}^{\delta_-(x-L)})$, with the spatial decay parameters $\delta_\pm$ maintaining consistency with the left boundary solutions. Analysis of the analytical expressions for $\delta_\pm$ reveals that the critical condition $\Gamma_z - 2t_{\mathrm{s}} = 0$ induces $\delta_- = 0$, leading to complete hybridization of Ψ_{L} and Ψ_{R} with bulk states while simultaneously driving the system into a gapless phase. From the discussion above, we may have a clear understanding of the creation and annihilation of edge states when we alter the parameters t_{s}, t_{so}, and Γ_z. Building upon the preceding theoretical framework, our analysis focuses on the Hamiltonian in the vicinity of the Γ point. The generalized Hamiltonian described in Eq. (7) exhibits a quasiparticle excitation spectrum characterized by $E_\pm = \pm\sqrt{(\Gamma_z - 2t_{\mathrm{s}}\cos k)^2 + 4t_{\mathrm{so}}^2\sin^2 k}$. When $E_\pm = 0$, we have

$$\mathrm{e}^{\mathrm{i}k_\pm} = \beta_\pm = (\Gamma_z \pm \sqrt{\Gamma_z^2 - 4t_{\mathrm{s}}^2 + 4t_{\mathrm{so}}^2})/(2t_{\mathrm{s}} + 2t_{\mathrm{so}}),$$
$$\mathrm{e}^{-\mathrm{i}k_\pm} = \beta_\pm = (\Gamma_z \pm \sqrt{\Gamma_z^2 - 4t_{\mathrm{s}}^2 + 4t_{\mathrm{so}}^2})/(2t_{\mathrm{s}} + 2t_{\mathrm{so}}),$$

where $\Gamma_z - 2t_{\mathrm{s}}\cos k = 2\mathrm{i}t_{\mathrm{so}}\sin k$ and $\Gamma_z - 2t_{\mathrm{s}}\cos k = -2\mathrm{i}t_{\mathrm{so}}\sin k$ are employed respectively, except the real numbers $k = 0$ and $\pm\pi$. By employing the methodology utilized in the vicinity of the Γ point, we can analogously obtain edge states localized at both the left and right boundaries as $\psi'_{\mathrm{L}} = [1, 1]\,[(\beta_+)^x - (\beta_-)^x]$ and $\psi'_{\mathrm{R}} = [-1, 1]\,[(\beta_+)^{(L-x)} - (\beta_-)^{(L-x)}]$, where $\Gamma_z - 2t_{\mathrm{s}}\cos k = 2\mathrm{i}t_{\mathrm{so}}\sin k$ and $\Gamma_z - 2t_{\mathrm{s}}\cos k = -2\mathrm{i}t_{\mathrm{so}}\sin k$ are also adopted respectively. Furthermore, our findings demonstrate consistency with the previous study.[28] To elucidate the behavior of edge states across two distinct topological regimes,

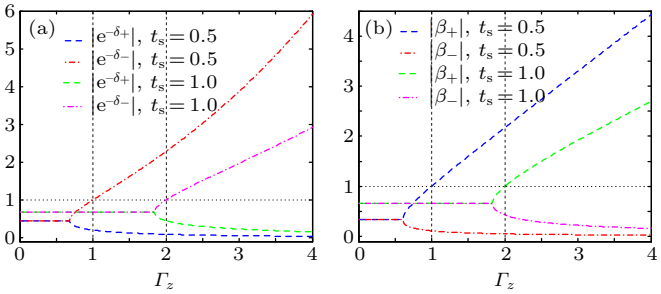


Fig. 2. Panels (a) and (b) show that $\left|\mathrm{e}^{-\delta_\pm}\right|$ and $|\beta_\pm|$ are less than 1 respectively when $\Gamma_z < 2t_{\mathrm{s}}$. There are topological edge states when $\Gamma_z < 2t_{\mathrm{s}}$. The parameters are $\{t_{\mathrm{so}} = 0.8t_{\mathrm{s}}, t_{\mathrm{s}} = 0.5\}$ and $\{t_{\mathrm{so}} = 0.4t_{\mathrm{s}}, t_{\mathrm{s}} = 1.0\}$.

figures 2(a) and 2(b) present the variations of $\left|e^{-\delta_\pm}\right|$ and $|\beta_\pm|$ as functions of Γ_z and t_s. As shown in Fig. 2, it is evident that there are edge states when $\Gamma_z < 2t_s$, whereas no edge states exist when $\Gamma_z > 2t_s$.

It has been noted that when the AIII class topological insulator is coupled to an s-wave superconductor by the proximity effect, it can become a BDI class topological superconductor. On the Nambu basis $(c_{k\uparrow}, c_{k\downarrow}, c^+_{-k\uparrow}, c^+_{-k\downarrow})$, its Hamiltonian is[29]

$$\begin{aligned} H_{\rm BDI}(k) &= (\Gamma_z - 2t_s\cos k)\,\sigma_z\tau_z \\ &\quad + 2t_{so}\sin k\sigma_y\tau_z + \Delta\sigma_y\tau_y, \end{aligned} \tag{11}$$

where σ_i and τ_i are Pauli matrices in the spin and particle–hole space respectively and Δ is the s-wave pairing gap. It is well established that the topological-invariant $N_{\rm BDI}$ assumes distinct values under specific parameter regimes: $N_{\rm BDI} = 2$ when $2t_s - \Gamma_z > \Delta$; $N_{\rm BDI} = 1$ when $|\Gamma_z - 2t_s| < \Delta$; and $N_{\rm BDI} = 0$ when $\Gamma_z - 2t_s < \Delta$.[29] In the vicinity of the Γ point, the Hamiltonian $H_{\rm BDI}(k)$ can be expressed in the following form:

$$\begin{aligned} H_{\rm BDI}(k\to 0) &= \left(\Gamma_z - 2t_s + t_s k^2\right)\sigma_z\tau_z \\ &\quad + 2t_{so}k\sigma_y\tau_z + \Delta\sigma_y\tau_y. \end{aligned} \tag{12}$$

Through diagonalization of the aforementioned Hamiltonian $H_{\rm BDI}(k\to 0)$, the accurate quasiparticle excitation spectrum can be derived

$$E(k) = \pm\sqrt{\left(t_s k^2 + \Gamma_z - 2t_s \pm \Delta\right)^2 + 4t_{so}^2 k^2}. \tag{13}$$

In addition to the scenarios where $k = 0$ and $\Gamma_z - 2t_s \pm \Delta = 0$, which signify the conditions for gap closure and the boundaries of quantum phase transitions, there exist additional solutions under the zero-energy condition ($E(k) = 0$). These solutions are given by $-ik_{l\pm} = \gamma_{l\pm} = (t_{so} \pm \sqrt{t_{so}^2 + t_s(\Gamma_z - 2t_s + (-1)^l\Delta)})/t_s$ and $ik_{l\pm} = \gamma_{l\pm} = (t_{so} \pm \sqrt{t_{so}^2 + t_s(\Gamma_z - 2t_s + (-1)^l\Delta)})/t_s$ where $\{l = 1,2\}$ and we have utilized $\Gamma_z - 2t_s \pm \Delta = 2it_{so}$ and $\Gamma_z - 2t_s \pm \Delta = -2it_{so}$ respectively. To investigate edge states in the topological invariant regime characterized by $N_{\rm BDI} = 2$, we analyze the following equation:

$$H_{\rm BDI}(k\to 0)\psi = 0. \tag{14}$$

After some detailed demonstrations, we can arrive at $\psi_1 = [1,1,1,1]$, $\psi_2 = i[1,1,-1,-1]$, $\psi_3 = i[1,-1,-1,1]$, and $\psi_4 = [1,-1,1,-1]$ where we have taken advantage of $\Gamma_z - 2t_s - \Delta = 2it_{so}$, $\Gamma_z - 2t_s + \Delta = 2it_{so}$, $\Gamma_z - 2t_s - \Delta = -2it_{so}$ and $\Gamma_z - 2t_s + \Delta = -2it_{so}$ respectively. Consequently, the edge states localized at the left boundary $x = 0$ can be expressed as: $\Psi_1 = [1,1,1,1](e^{-\gamma_{1+}x} - e^{-\gamma_{1-}x})$ and $\Psi_2 = i[1,1,-1,-1](e^{-\gamma_{2+}x} - e^{-\gamma_{2-}x})$ with analogous expressions for the right boundary $x = L$: $\Psi_3 = i[1,-1,-1,1](e^{\gamma_{1+}(x-L)} - e^{\gamma_{1-}(x-L)})$ and $\Psi_4 = [1,-1,1,-1](e^{\gamma_{2+}(x-L)} - e^{\gamma_{2-}(x-L)})$. These results exhibit remarkable consistency with established theoretical frameworks.[29] Our analysis proceeds to the Hamiltonian given in Eq. (11), which enables derivation of the quasiparticle dispersion relation through diagonalization $E_\pm = \pm\sqrt{(\Gamma_z - 2t_s\cos k + (-1)^l\Delta)^2 + 4t_{so}^2\sin^2 k}$ where $\{l = 1,2\}$. When $E_\pm = 0$, we have $e^{ik_{l\pm}} = \eta_{l\pm} = \{(\Gamma_z + (-1)^l\Delta) \pm \sqrt{(\Gamma_z + (-1)^l\Delta)^2 - 4t_s^2 + 4t_{so}^2}\}/(2t_s + 2t_{so})$ and $e^{-ik_{l\pm}} = \eta_{l\pm} = \{(\Gamma_z + (-1)^l\Delta) \pm \sqrt{(\Gamma_z + (-1)^l\Delta)^2 - 4t_s^2 + 4t_{so}^2}\}/(2t_s + 2t_{so})$ where $\{l = 1,2\}$ and we have used $\Gamma_z - 2t_s\cos k \mp \Delta = 2it_{so}\sin k$ and $\Gamma_z - 2t_s\cos k \mp \Delta = -2it_{so}\sin k$ respectively, aside from $k = 0$ and $\pm\pi$. By employing the method utilized in the vicinity of the Γ point, the edge states localized at the left boundary $x = 0$ can be expressed as: $\Psi_1' = [1,1,1,1][(\eta_{1+})^x - (\eta_{1-})^x]$ and $\Psi_2' = i[1,1,-1,-1][(\eta_{2+})^x - (\eta_{2-})^x]$ and with corresponding states at the right boundary $x = L$: $\Psi_3' = i[1,-1,-1,1][(\eta_{1+})^{(L-x)} - (\eta_{1-})^{(L-x)}]$ and $\Psi_4' = [1,-1,1,-1][(\eta_{2+})^{(L-x)} - (\eta_{2-})^{(L-x)}]$. Systematic variation of parameters $\{t_s, \Gamma_z, \Delta\}$ enables the tracking of edge state creation and annihilation mechanisms across three distinct regimes, through quantitative analysis of the analytical norms $|e^{\gamma_{l\pm}}|$ and $|\eta_{l\pm}|$ shown in Figs. 3(a)–3(d).

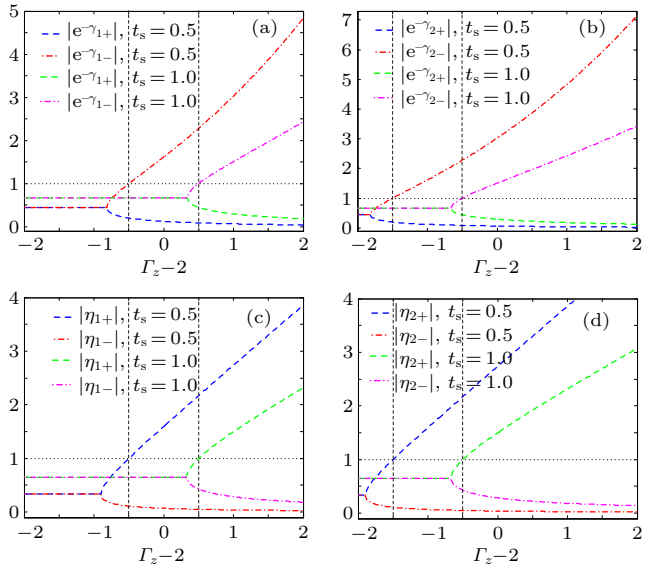


Fig. 3. When $2t_s - \Gamma_z > \Delta$, Panels (a)–(d) show the presence of topological edge states, as the absolute values of all decay coefficients are less than 1. However, when $|\Gamma_z - 2t_s| < \Delta$, only panels (a) and (c) present the existence of edge states, as the absolute values of all decay coefficients are below 1. In other cases, panels (a)–(d) illustrate the absence of edge states, given that the absolute values of all decay coefficients exceed 1. The parameters are $\{t_{so} = 0.8t_s, \Delta = t_s, t_s = 0.5\}$ and $\{t_{so} = 0.4t_s, \Delta = 0.5t_s, t_s = 1.0\}$.

5. Example III: A similar spinless $p_x \pm ip_y$ superconductor

We consider a theoretical model that hosts localized Majorana fermion states on the surface of a topological insulator.[30] In the Nambu notation $\left(\psi_\uparrow, \psi_\downarrow, \psi^+_{-\uparrow}, -\psi^+_{-\downarrow}\right)$, its

Hamiltonian is given

$$H = -\mathrm{i}\upsilon\tau_z\boldsymbol{\sigma}.\boldsymbol{\nabla} - \mu\tau_z + \Delta_0(\tau_x\cos\phi + \tau_y\sin\phi), \quad (15)$$

where τ_i and σ_i are Pauli matrices and μ is the chemical potential. In this analysis, we restrict consideration to the parameter regime with $\mu = 0$ due to its maximal computational tractability. When $\Delta = \Delta_0\mathrm{e}^{\mathrm{i}\phi}$ is spatially homogeneous, diagonalization of the Hamiltonian H yields the excitation spectrum $E_\pm(k) = \pm\sqrt{\upsilon^2k^2 + \Delta_0^2}$. It is worth mentioning that the momentum-dependent pairing amplitude (k) serves as the essential control parameter for inducing topological phase transitions. Furthermore, the Hamiltonian is systematically analyzed in polar momentum space to exploit rotational symmetry. Constructing solutions to the eigenvalue equation $H\psi = 0$ within the momentum-space framework, where the pairing field adopts the vortex-phase ansatz $\Delta = \Delta_0(k)\mathrm{e}^{\pm\mathrm{i}\theta}$, we derive topologically protected zero-energy states localized at the vortex core through our proposed approach. When $\Delta = \Delta_0\mathrm{e}^{-\mathrm{i}\theta}$, we have $\psi_- = [1,0,0,-\mathrm{i}]\mathrm{e}^{-\int_0^r \mathrm{d}r'\Delta_0(r')/\upsilon}$ and analogously $\psi_+ = [0,\mathrm{i},1,0]\mathrm{e}^{-\int_0^r \mathrm{d}r'\Delta_0(r')/\upsilon}$ for $\Delta = \Delta_0\mathrm{e}^{\mathrm{i}\theta}$ where we have also employed the relation $\upsilon k = \mathrm{i}\Delta_0$ and $\upsilon k = -\mathrm{i}\Delta_0$ respectively, compatible with established theoretical predictions.[30] Furthermore, to validate the accuracy of the proposed method, we have also computed the edge states in the quantum anomalous Hall effect within 2D transition metal oxides. Our findings are in agreement with prior research outcomes.[31] Since the calculation process and results are similar to those of the spinless superconductor, we will not elaborate on the specific details here. From the examples of topological and non-topological edge/surface states discussed above, if the Hamiltonian of the studied system exhibits a relatively simple form or its band structure possesses specific symmetry properties (e.g., symmetry about $E = 0$), the approach we have proposed demonstrates significant practical applicability.

6. Conclusion and perspectives

In summary, we have developed a method for determining the edge/surface states of bounded systems by analyzing the bulk Hamiltonian of their corresponding unbounded systems. This approach involves extending the real k-space to the complex k-one, thereby rendering the Hamiltonian non-Hermitian. Our method successfully reveals the fundamental characteristics of the bulk–boundary correspondence: edge/surface states exhibiting exponential decay in the bounded systems are inherently embedded within their corresponding unbounded systems. If the behavior of edge/ surface states exhibits the fundamental correlation with the boundaries, these states cannot manifest without appropriate boundary conditions stemming from wave function convergence requirements. The analytical findings establish an intrinsic relationship between the localized edge/surface states in bounded systems and their corresponding bulk Hamiltonians. However, this interconnection requires more rigorous investigation to elucidate its fundamental mechanisms.

Appendix A

At the level of the next nearest neighbor hopping approximation and within the basis of $(c_{k\mathrm{A}}, c_{k\mathrm{B}})$, its Hamiltonian reads (see Fig. 1(a) in the text)

$$H = \begin{pmatrix} n & m \\ m^* & n \end{pmatrix}, \quad (A1)$$

where

$$\begin{cases} m = t(\exp(\mathrm{i}k_xa/\sqrt{3}) + 2\cos(k_ya/2)\exp(-\mathrm{i}k_xa/2\sqrt{3})), \\ n = s(4\cos(k_ya/2)\cos(\sqrt{3}k_xa/2) + 2\cos(k_ya)), \end{cases}$$

t and s denote the nearest neighbor hopping parameter and the next nearest neighbor hopping parameter, respectively. By diagonalizing H, we can obtain the bulk energy spectrum $E_\pm(k) = n \pm |m|$. We focus on zero-energy edge states in the armchair edged graphene where k_x is a good quantum number. When $E_\pm(k) = 0$, we obtain the legitimate solutions $\mathrm{e}^{\mathrm{i}k_\pm a/2} = -z \pm \sqrt{z^2-1}$ and $\mathrm{e}^{-\mathrm{i}k_\pm a/2} = -z \pm \sqrt{z^2-1}$ where $n = |m|$ and $n = -|m|$ are employed respectively and

$$\begin{cases} z = y_j^{(i)}, \quad x_\pm = \dfrac{t^2 \pm \sqrt{t^4 + 12s^2t^2}}{2s^2}, \\ y_\pm^{(i)} = \dfrac{-2\cos\left(\dfrac{\sqrt{3}k_xa}{2}\right) \pm \sqrt{4\cos^2(\dfrac{\sqrt{3}k_xa}{2}) + 2(2+x_i)}}{2}, \\ i = +\,(-), \quad j = +\,(-). \end{cases}$$

By conducting a comparative analysis of the calculation results obtained under the nearest neighbor and next nearest neighbor approximations, we observe that $\{\mathrm{e}^{\mathrm{i}k_\pm a/2}, \mathrm{e}^{-\mathrm{i}k_\pm a/2}\}$ exhibit a high degree of similarity in their mathematical expression forms. On this basis, we can reach a consistent conclusion: zero-energy edge states are absent in the armchair edged graphene.

Acknowledgements

Project supported by the National Natural Science Foundation of China (Grant No. 11847061) and the Domestic Visiting Program for Young and Middle-aged Teachers in Shanghai Universities.

References

[1] Meier D, *et al*. 2012 *Nat Mater.* **11** 284
[2] Seidel J, *et al*. 2009 *Nat Mater.* **8** 229
[3] Waser R and Rüdiger A 2004 *Nat. Mater.* **3** 81
[4] Kane C L and Mele E J 2005 *Phys. Rev. Lett.* **95** 146802
[5] Kane C L and Mele E J 2005 *Phys. Rev. Lett.* **95** 226801
[6] Bernevig B A, Hughes T L and Zhang S C 2006 *Science* **314** 1757
[7] Liu C, Hughes T L, Qi X L, Wang K and Zhang S C 2008 *Phys. Rev. Lett.* **100** 236601

[8] Hatsugai Y 1993 *Phys. Rev. Lett.* **71** 3697
[9] Hatsugai Y 1993 *Phys. Rev. B* **48** 11851
[10] Lu L, Joannopoulos J D and Soljačić M 2014 *Nat. Photon.* **8** 821
[11] Sarma S D, Freedman M and Nayak C 2015 *npj Quantum Inf.* **1** 15001
[12] Blanco-Redondo A, Bell B, Oren D, Eggleton B J and Segev M 2018 *Science* **362** 568
[13] Kang J, Liu T, Yan M, *et al*. 2023 *Laser Photon. Rev.* **17** 2200499
[14] Shan W Y, Lu H Z and Shen S Q 2010 *New J. Phys.* **12** 043048
[15] Qiao Z, Jiang H, Li X, Yao Y and Niu Q 2012 *Phys. Rev. B* **85** 115439
[16] Qiao Z, *et al*. 2010 *Phys. Rev. B* **82** 161414
[17] Yang Y, Xu Z, Sheng L, Wang B, Xing D Y and Sheng D N 2011 *Phys. Rev. Lett.* **107** 066602
[18] Bender C M and Boettcher S 1998 *Phys. Rev. Lett.* **80** 5243
[19] Wang H P, Ren L, Qin L G and Qiu Y 2020 *J. Phys. Soc. Jpn.* **89** 074705
[20] Wang H P, Ren L, Qin L G and Qiu Y 2021 *Chin. Phys. B* **30** 107301
[21] Wang H P, Ren L, Zhang X L and Qin L G 2024 *Chin. Phys. B* **33** 107302
[22] Lee D H and Joannopoulos J D 1981 *Phys. Rev. B* **23** 4988
[23] Zhao Y Y, Li W and Tao R B 2012 *Chin. Phys. B* **21** 027302
[24] Slager R J, Mesaros A, Juričić V and Zaanen J 2013 *Nat. Phys.* **9** 98
[25] García-Fuente A, Carrascal D, Ross G and Ferrer J 2023 *Phys. Rev. B* **107** 115403
[26] Zhao Y Y, Li W and Tao R B 2012 *Physica B* **407** 724
[27] Wang H P, Gao T and Tao R B 2015 *Sci. Rep.* **5** 8679
[28] Liu X J, Liu Z X and Cheng M 2013 *Phys. Rev. Lett.* **110** 076401
[29] He James J, Wu J, Choy T P, Liu X J, Tanaka Y and Law K T 2014 *Nat. Commun.* **5** 3232
[30] Fu L and Kane C L 2008 *Phys. Rev. Lett.* **100** 096407
[31] Wang H P, Luo Wei and Xiang H J 2017 *Phys. Rev. B* **95** 125430